Frontiers in Bioscience Landmark

Front. Biosci. (Landmark Ed) **2022**; 27(4): 131
https://doi.org/10.31083/j.fbl2704131

Original Research

Autologous Mesenchymal Stromal Cells Combined with Gelatin Sponge for Repair Intervertebral Disc Defect after Discectomy: A Preclinical Study in a Goat Model

Qiuming Yuan[1,2,†], Lilong Du[1,3,†], Haiwei Xu[1,†], Kaihui Zhang[1], Qifeng Li[3], Hao Zhang[3], Yue Liu[1], Xinlong Ma[1], Baoshan Xu[1,3,*]

[1]Department of Minimally Invasive Spine Surgery, Tianjin Hospital, Tianjin University, 300211 Tianjin, China
[2]Department of Spine and Joint Surgery, Tianjin Baodi Hospital, Baodi Clinical College of Tianjin Medical University, 301800 Tianjin, China
[3]Graduated School of Tianjin Medical University, 300070 Tianjin, China
*Correspondence: xubaoshan99@126.com (Baoshan Xu)
[†]These authors contributed equally.
Academic Editor: Pietro Gentile
Submitted: 8 December 2021 Revised: 3 March 2022 Accepted: 8 March 2022 Published: 19 April 2022

Abstract

Background: The defect of intervertebral disc (IVD) after discectomy may impair tissue healing and predispose patients to subsequent IVD degeneration, which is thought to be an important cause of recurrence. Cell-based approaches for the treatment of IVD degeneration have shown promise in preclinical studies. However, most of these therapies have not been approved for clinical use due to the risks of abnormal differentiation and microorganism contamination of the culture-expanded cells. Selective cell retention (SCR) technology is non-cultivation technique, which can avoid those preambles in cell expansion. In this study, we used a commercially available BONE GROWTH PROMOTER device (BGP, FUWOSI, Chongqing, China) to concentrate mesenchymal stromal cells (MSCs) from bone marrow aspirate (BMA) through SCR technology. **Methods**: A small incision was made on the L2/3, L3/4 and L4/5 discs of goats and part of nucleus pulposus (NP) was removed to construct IVD defect model. The L2/3 disc was subjected to discectomy only (DO group), the L3/4 disc was implanted with enriched BMA-matrix (CE group), and the L4/5 disc was implanted cultured autologous bone marrow MSCs matrix (CC group). And the intact L1/2 disc served as a non-injured control (NC group). The animals were followed up for 24 weeks after operation. Spine imaging was analysis performed at 4 and 24 weeks. Histology, immunohistochemistry, gene expression and biomechanical analysis were performed to investigate the IVD morphology, content and mechanical properties at 24 weeks. **Results**: The CE and CC groups showed a significantly smaller reduction in the disc height and T2-weighted signal intensity, and a better spinal segmental stability than DO group. Histological analysis demonstrated that CE and CC groups maintained a relatively well-preserved structure compared to the DO group. Furthermore, real-time PCR and immunohistochemistry demonstrated that aggrecan and type II collagen were up-regulated in CE and CC groups compared to DO group. **Conclusions**: The strategy of MSCs enrichment combined with gelatin sponge by SCR technology provides a rapid, simple, and effective method for cell concentration and cell-carrier combination. This reparative strategy can be used in clinical treatment of IVD defect after discectomy. **Clinical Trial Registration**: NCT03002207.

Keywords: intervertebral disc; discectomy; regeneration; mesenchymal stromal cells; selective cell retention; gelatine tissue scaffolds

1. Introduction

Intervertebral disc (IVD) degeneration (IVDD) is a common disease that can lead to low back pain, nerve compression and disability. Lumbar disc herniation (LDH) with radiculopathy is one of the most common IVDD-linked clinical diseases, which causes huge socioeconomic burden in the world. The treatment of severe LDH often requires surgical approach [1]. Discectomy remains the classic surgical procedure for treating LDH, which consists of removal of the herniated part of nucleus pulposus (NP) to relieve radicular pain. However, despite alleviating pain and improving function, 20%–25% of patients experience long-term unsatisfactory outcomes [2,3]. The main reason is that the IVD defect after discectomy failed to spontaneous repair, which can result in progressive IVDD, a loss of disc height and even LDH recurrence. Decreased disc height can lead to reduced range of motion.

Several attempts have been made to seal IVD defects by sutures or rigid buttress devices. Bailey *et al*. [4] used an FDA-approved X-close device to suture open annulus fibrosus (AF) defect after discectomy. In addition to sutures there are currently commercial annular closure devices such as Barricaid implant and Inclose Mesh [5,6], which can block off the IVD defect by forming a mechanical barrier. However, these repair techniques focus on closing the wound of defect without functional restoration of the IVD and some scholars found the additional AF repair had no significant superiority [4,7]. Repair methods ideally need to provide both functional restoration and induce IVD regeneration. This makes biologically active tissue scaffold methods attractive options [8]. Therefore, a biological repairing method for IVD defect is needed.

Advances in cell-based therapy and tissue engineering have led to significant progress in the field of regenerative medicine for IVD regeneration. Various cell type and source, including IVD-derived cells and multipotent cells, have been proven to delay the progressive degenerative process [9–11]. Mesenchymal stromal cells (MSCs) are a convenient cell source with translational advantages [12]. Several reports have described the application of MSCs, including bone marrow-derived MSCs (BM-MSCs), adipose-derived MSCs (ASCs) and umbilical cord-derived MSCs (UC-MSCs), to repair and regenerate the damaged IVD in preclinical and clinical studies [13–15]. In recent years, many completed and ongoing clinical trials testing the efficacy of cell-based therapies for regeneration IVD [16–21]. In clinical trials, Yoshikawa *et al*. [22] reported that using cultured autologous BMSCs combined with gelatin sponge repairing the degenerated IVD could significantly reduce the pain symptoms and increase the IVD water content. However, most of the preclinical and clinical studies used culture-expanded cells for transplantation, with the risk of differentiate abnormality and complex steps which is time consuming and difficult for clinical application. Bone marrow aspirate (BMA) is considered an important source of MSCs in both clinical and experimental studies [23]. Unfortunately, the MSCs represent a very small fraction of about 0.001–0.01% of nucleated cell count of the BMA [24–26], leading to a limited therapeutic effect. Selective cell retention (SCR) technology could concentrate target cells (including stem and progenitor cells) and effective components from BMA into a carrier material to facilitate the rapid attachment of nucleated cells, which holds great potential for cell preparation.

In terms of IVDD model, previous studies have established in small and large animal models, including rats, rabbits, sheep [27,28], goat [29], mini-pigs [30] and canine [31,32], which was induced mechanically, enzymatically or surgically by puncture or incision of the AF with or without nucleotomy, or by injection of biochemical agents for extracellular matrix degraded. Recently, larger sized AF defect or IVD defect model after annulotomy with or without nucleotomy was established and used to study the repair of IVD. To the authors knowledge discectomy-associated defects are more common clinically and need to be repaired. Therefore, it is necessary to construct a suitable animal model where discectomy has been performed to mimic the conditions in human IVDs after discectomy.

The gelatin sponge was widely used in spine surgery, with the advantage of high histocompatibility, high plasticity and absorbability. The gelatin sponge could be used safely as cell carrier for disc regeneration therapy and AF defect repair [22,33]. In this study, we performed a preclinical study that gelatin sponge combine with autologous cultured BMSCs or enriched BMA were transplanted into NP defect, followed by suturing and sealing AF to repair IVD defect after discectomy in a goat model. We hypothesized that this treatment could repair the IVD defect and retard disc degeneration. Our secondary aim was to compare the repair efficacy between BMA concentrate and cultured BMSCs.

2. Materials and Methods

2.1 Study Design

A total of 15 goats (female, 24 months, 48.3 $\pm$ 3.6 kg), were used in this study. All goats were healthy and received X-ray and Magnetic Resonance Imaging (MRI) scans to assure the absence of IVDD-related diseases before the study. All goats were fasted for 24 h before surgery. Five goats were randomly selected, and the BMA was aspirated from the iliac crest for enrichment to determine the effect of the BONE GROWTH PROMOTER (BGP, FUWOSI, Chongqing, China), as a SCR technology using negative pressure to facilitate the permeation of the biomaterials by bone marrow under conditions of aspiration [25,34–36]. The remaining 10 goats were used for IVD defect repair. BMA aspirated from randomly one side of iliac crest was cultured to obtain autologous BMSCs, and then the autologous BMSCs combined with gelatin sponge matrix were implanted into the IVD defect; the autologous BMA aspirated from the other side of the iliac crest was enriched by BGP and implanted into IVD after discectomy. The goats were euthanized 24 weeks after operation to compare the repair effect of the two methods (Fig. 1).

2.2 Bone Marrow Aspirate and Enrichment

Five goats were anesthetized by intramuscular injection of atropine (0.01 mL/kg) and intravenous injection of 3% pentobarbital sodium (1 mL/kg). The BMA was aspirated from iliac crest of the goat using a 16 G bone marrow puncture needle, which was rinsed with 1000 U/mL heparin to prevent coagulation (Fig. 2A). Two puncture holes were made at one side iliac crest, and 10 mL BMA was aspirated from each hole [37]. For preparation of the enriched BMA-matrix grafts, two pieces of gelatin sponge (60 mm $\times$ 20 mm $\times$ 5 mm, XiangEn Medical Technology Development Co. Ltd, Nanchang, China) were chopped into small cubes (5 mm $\times$ 5 mm $\times$ 2.5 mm), and were loaded into the BGP (Fig. 2A). Then, a total of 20 mL BMA aspirated from one side iliac crest was injected into the BGP for enrichment (**Supplementary Fig. 2A–D**). Slowly press the handle of the BGP to the end to send the BMA into the conical cup filled with gelatin sponge, release the handle to automatically rise, and form a negative pressure at the bottom of the conical cup to draw the BMA back into the tube, and repeat the above operation for 5 times. Five cycles were processed until MSCs and effective constituent in BMA were fully filtered and seeded into the gelatin sponge cubes.

The enriched BMA-matrix was taken out and fixed in 4% paraformaldehyde for 12 h. After gradient ethanol dehydration and critical point drying, the sample and gelatin sponge was cut into 1 mm slices and pasted on the carrier

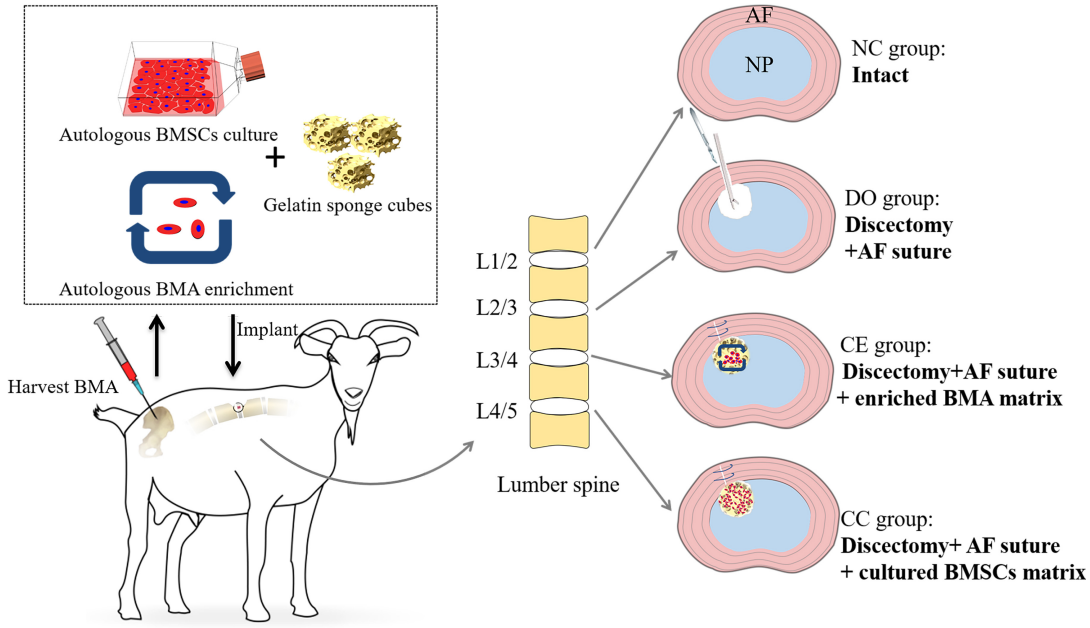

Fig. 1. Schematic illustration of the study design of *in vivo* repair IVD defect after discectomy at goat model.

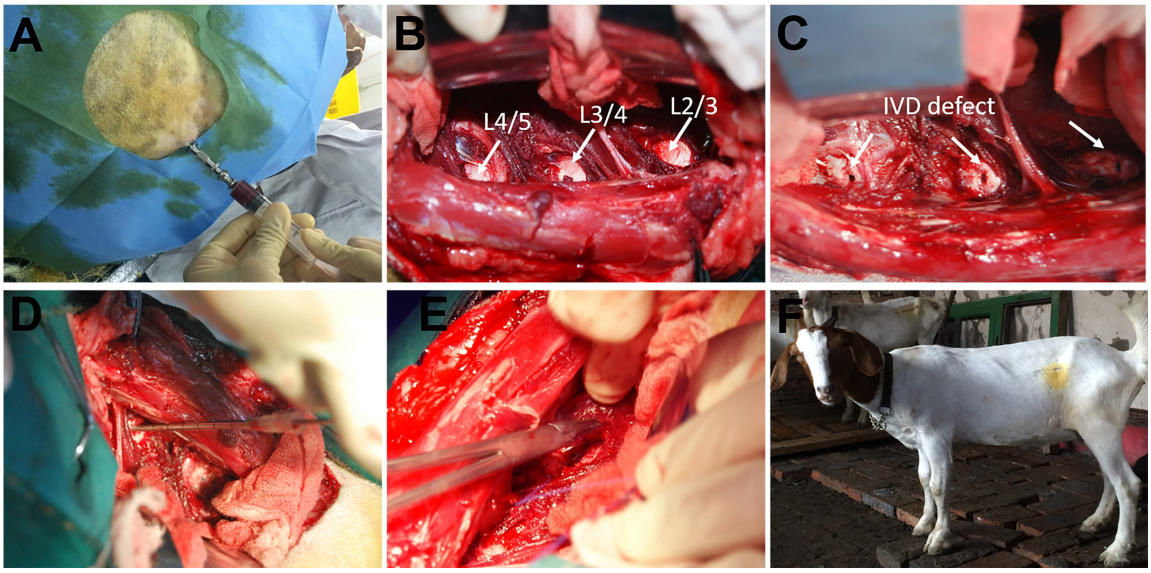

Fig. 2. Surgical approach. (A) The BMA was aspirated from the ilium crest of goat. (B) Exposure of the IVD. (C) Construction of IVD defect model after discectomy (arrow). (D) Graft implantation. (E) Sutured annulus fibrosus. (F) All animals recovered from the procedure without complication and retained full lumbar spine function.

table with conductive tape, respectively. The surfaces were sprayed with gold and observed by scanning electron microscope (SEM, Quanta 200, Fei, Hillsboro, OR, USA).

To assess the enrichment effect, the volume of BMA was measured before and after enrichment process, and the samples were taken for flow cytometry (FACS Aria III, BD Corporation, Franklin Lakes, NJ, USA) to detect the number of nucleated cells and the number of the target cells with negative expression of CD34 and CD45 and positive expression of CD90. The number and concentration of cells in the BMA before and after BMA enrichment using BGP were assessed by flow cytometry. The steps are as follows: (1) Take three samples of BMA before and after enrichment, isotype and corresponding isotype control, and put 300 μL of each sample into a tuber. (2) Add CD34, CD45, CD90 and CD34-FITC, CD45-PEcy^{TM}7, CD90-PE (BD Corporation, Franklin Lakes, NJ, USA) to the corresponding tuber according to the antibody instructions and flow cytometry requirements. Incubate in a 37 °C incubator protected from light for 20 min. (3) Add 1.5 mL erythrocyte lysate to each

tube for 10 min in the dark. Centrifuge at 400 g for 10 min and discard the red supernatant. If there are still many red blood cells, repeat the above operation. (4) Wash twice with PBS (phosphate buffered saline) and resuspend with 500 μL PBS for flow cytometry detection. Then the concentration and adhesion multiple of the retention cells in the gelatin sponge matrix were calculated according to the calculation formula as follows: retention cells concentration = retention cells number/volume of retention fluid; cells adhesion multiple = the retention cells concentration/original BMA cells concentration [25].

Furthermore, 100 μL original BMA and a small amount of enriched matrix were cultured in a culture dish respectively with 10 mL of the DMEM/F12 culture medium (containing L-Glutamine and 10% FBS) for 11 days. In our study, there is all a penicillin-streptomycin solution in the culture medium, the concentration of penicillin is 100 U/mL, and the concentration of streptomycin is 0.1 mg/mL, and the culture conditions are all in an incubator with 20% oxygen and 5% carbon dioxide. Then, the cells adhered to the culture plate surface were identified by crystal violet stanning to assess the enrichment effect, followed by observation under microscope (Leica, DM3000, Wetzlar, Germany) [37].

2.3 Construction of Cultured BMSCs-Matrix Grafts

For isolation of BMSCs, 20 mL of BMA was collected from the iliac crest and mixed with 2 mL heparin (1000 U/mL). Bone marrow mononuclear cells were isolated by density-gradient centrifugation using lymphoprep [38]. The mononuclear cells were cultured for 4 days in a 100 cm^2 culture flask with DMEM/F12 culture medium containing 20% FBS. Adherent cells were considered to be BMSCs. When BMSCs were cultured to reach 80–90% confluence, they were passaged and seeded in DMEM/F12 with 10% FBS. BMSCs were identified by flow cytometry to analyze the stem cell surface markers of CD90, CD34, and CD45 and analyzed the multilineage capability of adipogenic, chondrogenic, and osteogenic differentiation.

To facilitate analysis of the tracking of transplanted BMSCs in IVD, the BMSCs were infected with lentivirus-GFP (catalog number: GV492, Shanghai Genechem Co., Ltd, China), a lentivirus vector expressing the green fluorescent protein (GFP) gene. BMSCs were cultured and washed with PBS, and infected with lentivirus-GFP at optimal multiple of infection (MOI = 1:10). After 3 days, GFP expression was observed using a fluorescence microscope (Leica, DMI4000, Wetzlar, Germany). 100 μL GFP-labeled autologous BMSCs of 1×10^6 passage 3 was seeded into gelatin sponge cubes to obtain cultured BMSCs-matrix grafts, which is prepared for intraoperative implantation of disc defects of three goats.

2.4 Surgical Procedure

The goats were general anesthetized by intramuscular injection of atropine (0.01 mL/kg) and xylazine hydrochloride (0.02 mL/kg). All animals receive perioperative intravenous antibiotic (ceftiofur sodium, 25 mg/kg). Once anaesthetized, the goat is placed on the operating table in the lateral position, and the operation area was shaved and disinfected routinely with iodophor. A longitudinal 10 cm incision parallel and 1 cm anterior to the transverse processes is made according to the desired discs level using a left lateral retroperitoneal approach [39]. The subcutaneous layers were dissected using monopolar cautery. With the thoracolumbar fascia divided, the retroperitoneal space can be entered. The psoas and quadratus lumborum muscles are retracted posterolaterally, by the assistant, using a retractor, and blunt separation of the muscles attached to the disc, further exposing the target discs (Fig. 2B). A small incision was made at the left-anterior surfaces of the L2/3, L3/4 and L4/5 discs with a sharp knife, and approximately 50 mg NP tissues was removed from a single disc with small NP forceps to construct IVD defect model (Fig. 2C). The L2/3 disc was subjected to discectomy only (DO group), the L3/4 disc was implanted with enriched BMA-matrix (CE group), and the disc L4/5 was implanted cultured BMSCs-matrix (CC group) (Fig. 2D). And the intact L1/2 disc served as a non-injured control (NC group). The AF incision was closed using an absorbable suture (Fig. 2E). Then hemostasis is achieved, and muscle, fascia and skin were separately sutured layer by layer. Strict sterile precautions are maintained at all times. The goat was awakened by benzoxazole hydrochloride injection (0.01 mL/kg IM). After operation, all goats received intramuscular injection of flunixin meglumine (0.2 mL/kg) for analgesia for three days. Dressing change regularly until healing of the incision site was complete. The animals were observed at least once daily for general health and appearance by the veterinary staff and carefully monitored for signs of pain, discomfort, gait or posture. The animals were followed up for 24 weeks after the operation.

2.5 Imaging Analysis (X-Ray Imaging and MRI)

Lumbar X-ray imaging of goats was performed under general anesthesia at pre-operation and 4, 24 weeks after operation. The change in IVD height was evaluated by the disc height index (DHI) [40,41]. Disc height and the adjacent vertebral body heights were measured on the midline and 25% of the disc's width from the midline on either side. The DHI was expressed as the mean of the 3 measurements from midline to the boundary of the central 50% of disc width divided by the mean of the 2 adjacent vertebral body heights. Changes in DHI were expressed as %DHI and were standardized to the preoperative DHI as follows: %DHI = ((postoperative DHI/preoperative DHI) $\times$ 100).

MR scans were obtained in T2-weighted images in all groups at pre-operation and 4, 24 weeks after operation in

the sagittal and axial planes using a 1.5 T scanner (GE, Boston, MA, USA). T2-weighted sections in the sagittal plane were obtained under the following settings: fast spin echo sequence with time to repetition of 2500 seconds and time to echo of 85 seconds; 384 (h) $\times$ 224 (v) matrix; field of view of 260; and four excitations. The section thickness was 3 mm with a 0.3 mm gap. The grayscale of the NP and the cerebrospinal fluid on T2-weighted sagittal MRI was determined by Image J version 1.51j8 (National Institutes of Health, MD, USA). The disc relative gray index (RGI) was calculated by dividing the gray value of the NP by the gray value of the cerebrospinal fluid [31]. The Pfirrmann classification scheme was applied to grade IVD degeneration [42]. All image assessments were performed by three independent observers who were blinded to the samples, and the mean of the three evaluations was recorded.

2.6 Biomechanical Analysis

Goats were sacrificed by intravenous injection of overdosed pentobarbital at 24 weeks after surgery, and the ten lumbar spines were harvested. Biomechanical testing was performed on the spinal motion segment with ligamentous attachments and muscles removed. The denture base resin embedding sample was vertically installed on the biomechanical machine (MTS 858 Bionix II, Maumee, IN, USA) for biomechanical testing. Every vertebra of L1-5 was marked by markers in the same position (the specific position of every vertebra), and the motion of the markers was recorded by 3D Dynamic Capture System Camera (NDI Corporation, Canada) from different direction (Fig. 3A). The fresh spinal specimens were kept wet during the process of testing. Preconditioning was repeated three times (30 seconds/time) with 1 N preloading. The multidirectional bending moments (flexion and extension ($\pm$3 N m, x axis), left and right bending ($\pm$3 N m, z axis), and left and right torsion ($\pm$3 N m, y axis) were applied to the head end of the sample, while the tail end of the sample remained fixed. The multidirectional range of motion (ROM) of individual motion segments of every IVD was measured three times respectively according to the motions of markers.

2.7 Macroscopic Observation and Histological Analysis of IVD

After the biomechanical testing, the L1/2, L2/3, L3/4, and L4/5 discs of nine goats selected randomly were cut transversally at the center of the NP for macroscopic evaluation. A previously published histological grading system was applied to assess disc degeneration [43,44]. Two histologists who were blinded to the samples performed evaluation of these sections, with their intra-observer error being minimum. One half of every disc was used for histological studies and identify the tracking transplanted cells in the NP tissues, and the other half was stored in liquid nitrogen (–196 ℃) for realtime PCR analysis of gene expression.

The remaining discs of one goat were isolated consisting of the total IVD and 0.5 cm of adjacent vertebral body and fixed in 4% paraformaldehyde for 5 days. Then the samples were decalcified in 15% EDTA for 6 months and subsequently embedded in paraffin. To visualize intact disc, the coronal sections of entire disc were cut using microtome (Leitzl516, Leica, Wetzlar, Germany) and stained with hematoxylin and eosin (H&E). To visualize histologic changes in NP tissue, NP tissues were fixed in 4% paraformaldehyde for 24 h and processed for paraffin embedding and sectioning into transversal sections (6 μm). The transversal sections were stained with H&E, Safranin O and Sirius Red for evaluation.

Immunohistochemistry was performed for Collagen II (II-II6B3, DSHB, Iowa City, IA, USA) and Aggrecan (ABT1373, Millipore, Burlington, AL, USA) analysis. Rehydrated sections were serially incubated at room temperature in proteinase K (Sigma, Hesse, Germany) for 5 min, 3% hydrogen peroxide for 10 min, blocking reagent for 5 min (BD5001, Bioworld Technology, Nanjing, China), and incubated with Collagen II (4 μL/mL) and Aggrecan (1:250 dilution) primary antibodies. After incubation at 4 ºC overnight, sections were incubated with antibody amplifier (BD5001, Bioworld Technology, Nanjing, China) for 10 min and horseradish peroxidase polymer for 10 min. Positive signal was visualized by diamino-benzidine (DAB). Finally, the sections were counterstained with hematoxylin, dehydrated and sealed. Then, the stained sections were observed under stereo-microscope (Leica, DM3000, Wetzlar, Germany).

2.8 Tracking of Transplated BMSCs in IVDs

To identify the existence of implanted cells in the NP tissues, the NP tissues were embedded in optimal cutting temperature (OCT) compound (Fisher Scientific, Pittsburgh, PA, USA) and sectioned at 6 μm. The GFP-positive cells were observed under fluorescence microscope (Leica, DMI4000, Wetzlar, Germany).

2.9 Gene Expression Analysis

Total RNA was extracted from the NP using the TRIspin [45]. After the cDNA had been obtained by reverse transcription using AMV reverse transcriptase (Takara, Beijing, China), relative gene expressions of Collagen I, Collagen II, Aggrecan and SOX-9 were determined by Real-time PCR (RT-PCR). GAPDH were applied as normalization control. The obtained cDNA was amplified by qPCR using SYBR Premix Ex Taq^{TM} (Takara, Beijing, China). A cycle threshold (Ct) value was obtained for each sample, and triplicate sample values were averaged. The $2^{-\Delta\Delta Ct}$ value was then used to calculate relative expression of each target gene [46]. The primers being used were listed in Table 1.

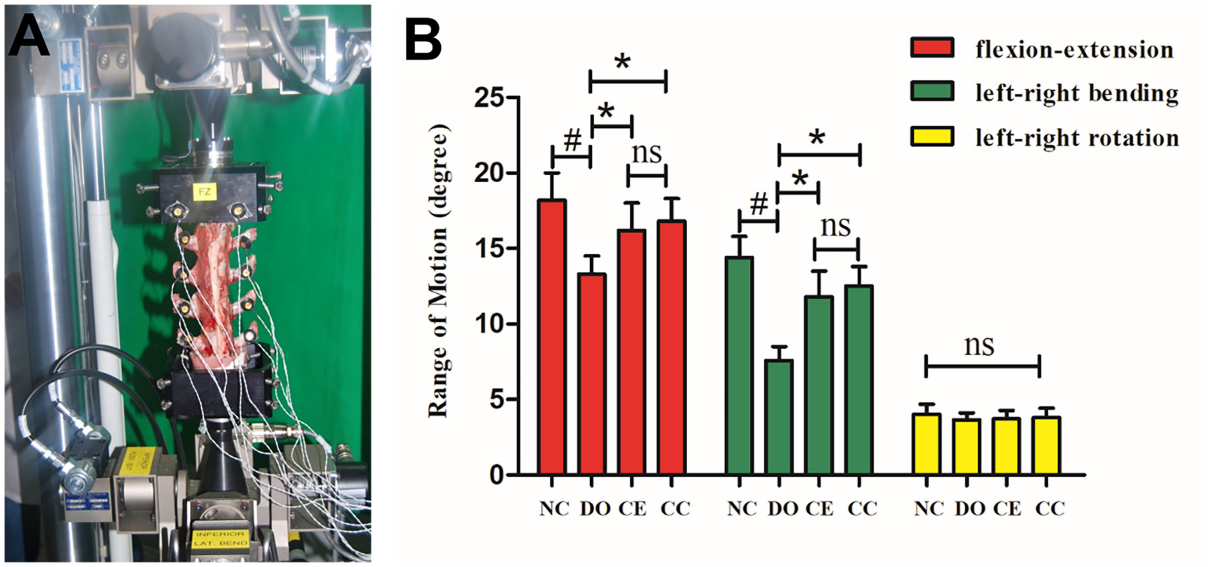

Fig. 3. Biomechanical analysis. (A) Spine specimens were tested in biomechanical tester. (B) The ROM of flexion-extension and left-right bending in the CE and CC groups were larger than that of the DO group at 24 weeks after operation. However, there was no significant difference in ROM between the CE and CC groups. ROM of left-right rotation was not statistically different in the four groups. All the data represent mean ± SD, n = 10. '#' refers to NC group compared to DO group. '*' refers to CE and CC groups compared to DO group respectively; #, *, = $p < 0.05$; ns, = $p > 0.05$.

Table 1. Primer sequences for RT-PCR.

Gene	Forward	Reverse
GAPDH	5′-GGCGTGAACCACGAGAAGTA-3′	5′-GGCGTGGACAGTGGTCATAA-3′
COL1A2	5′-CAAGGGAGATGCTGGTCCTG-3′	5′-TTCACCCTTAGCACCCACAG-3′
COL2A1	5′-CAACCCTGGAACTGACGGAA-3′	5′-ATACCAGGCTCACCCGTTTG-3′
ACAN	5′-GCAAGCTCCAGAAGCAAGTG-3′	5′-TCCACCAATGTCGTATCCACC-3′
SOX-9	5′-CACAAGAAGGACCACCCGGA-3′	5′-CACAAGAAGGACCACCCGGA-3′

2.10 Statistical Analysis

The statistical analyses were performed using SPSS version 24.0 software (IBM, Armonk, NY, USA). Data was assessed for normality using the Shapiro Wilks test. The radiograph measurements, biomechanical analyses, and RT-PCR analyses data were all fitted with normal distribution, and statistical analysis was performed using analysis of variance (ANOVA) and the Fisher's least significant difference post-hoc test. The MRI Pfirrmann grading and histological grading data did not conform to a normal distribution, and Kruskal Wallis H test was used for statistical analysis. Statistical significance was set at $p < 0.05$.

3. Results

3.1 Enrichment Effect and Identification of BMSCs

BMA was aspirated from 10 iliac crests of 5 goats for enrichment. After the BMA was enriched by the BGP, the adhesion multiple of nucleated cells and target cells was 6.40 ± 0.93 and 4.20 ± 0.65 respectively, which were measured respectively by flow cytometry (Fig. 4J).

BMSCs differentiation assay demonstrated the autologous BMSCs possess the capability of osteogenic, chondrogenic and adipogenic differentiation. (**Supplementary Fig. 1A–C**) Meanwhile, flow cytometry analysis showed the CD90 was positively expressed, and CD34 and CD45 were negatively expressed on the surface of the target cells, which was consistent with the BMSCs surface markers, indicating that BMSCs was successfully isolated and identified (**Supplementary Fig. 1D**).

3.2 Characteristics of Cells and Sponges

SEM images showed that the gelatin sponge was macroporous (Fig. 4B), and there were multiple round cells adhered to the porous wall of the enriched BMA matrix (Fig. 4C). After the BMA and the enriched BMA matrix were cultured for 11 days, crystal violet staining showed that there were a large number of colonies forming unit-fibroblast (CFU-F) at the bottom of the culture dish, and fusiform or polygonal cells were adherent to the wall. No bacterial growth was observed in all sample cultures (Fig. 4D,G). The results of flow cytometry detection and

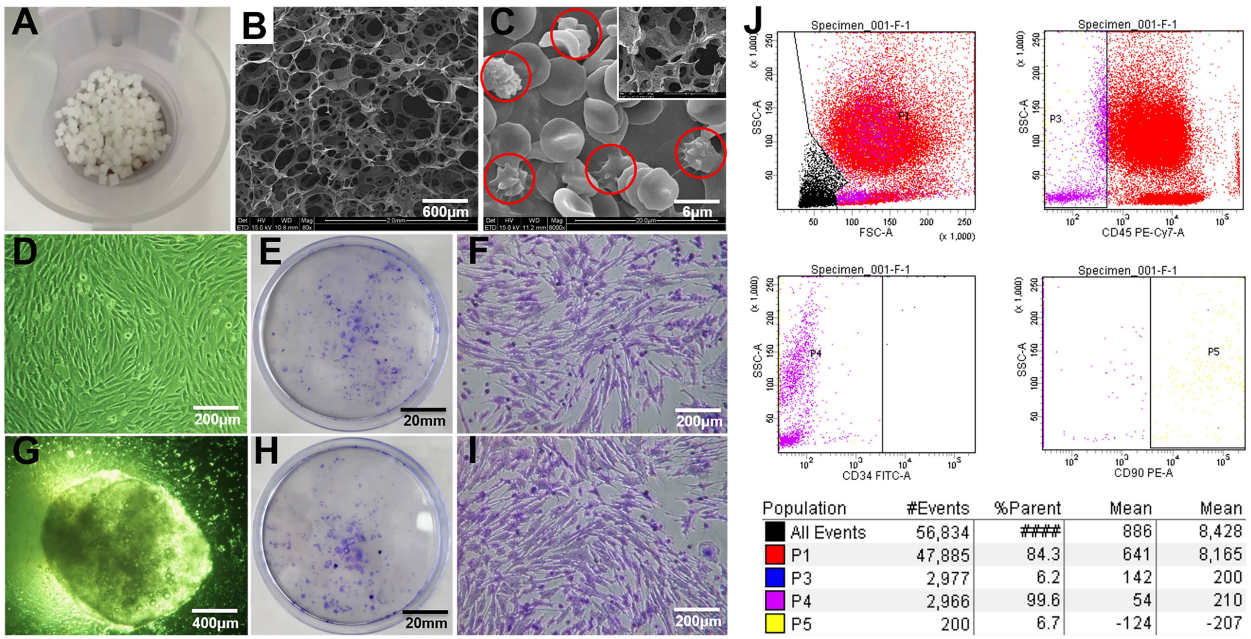

Fig. 4. Bone marrow enrichment. (A) Gelatin sponge cubes (5 mm × 5 mm × 2.5 mm) in the BGP. (B) SEM images shows the porous structure and their interconnection of gelatin sponge. (C) Multiple round cells adhered to the inner wall of the enriched matrix. The red circles indicate the nucleated cells. (D) After the BMA culturing for 11 days, the fibroblastic colony formation could be observed. (G) After the enriched BMA-matrix culturing for 11 days, a lot of cells were visible in and around the gelatin sponge. (E,H) Many colony-forming units stained by crystal violet in the culture dish of the BMA and the enriched matrix respectively. (F,I) Microscopic observation showed that a number of fusiform or polygonal cells stained by crystal violet were adherent to the bottom of culture dish from the BMA and the enriched matrix. respectively (×100). (J) The number of nucleated cells and target cells in the sample were detected by flow cytometry to calculate the adhesion multiple of the BGP. Calculation formula: adhesion multiple α = cells concentration of retentate/cells concentration of BMA. After the BMA enriched by the BGP, the adhesion times of the retained nucleated cells and the target cells were 6.40 ± 0.93 and 4.20 ± 0.65 respectively.

crystal violet staining showed that the MSCs in BMA could be effectively retained in gelatin sponge cubes by the BGP, and the cells viability were good.

3.3 General Remark of the Surgical Procedure

The mean weight of the NP removed from the DO, CE and CC group was 50.18 ± 3.95, 51.12 ± 5.38 and 51.26 ± 4.34 mg ($p > 0.05$), which indicated that the quantity of NP removed from each disc was consistent (**Supplementary Fig. 2E**). The average intraoperative blood loss was about 60 mL. The incisions of all goats were free of infection and healed smoothly. All goats successfully survived to the defined 24-weeks endpoint and showed no signs of neurological deficits or pain as determined by veterinary care staff.

3.4 Changes in the IVD Height and MRI Assessment

Radiographic analysis at 4 weeks after operation showed that the disc spaces in DO, CE and CC groups narrowed significantly, and the DO group continued to decrease at 24 weeks, while rate of decrease in the CE and CC groups slowed down after 4 weeks. With a mean DHI for NC group at beginning of the study expressed as 100%, the mean DHI of the DO, CE and CC group was 89.3 ± 3.3%, 89.7 ± 2.7% and 90.2 ± 2.5% at 4 weeks after surgery respectively ($p > 0.05$). The mean DHI of the CE and CC group was 82.0 ± 3.8% and 83.3 ± 3.2% at 24 weeks after surgery ($p = 0.503$), and all were higher than 68.3 ± 3.4% of the DO group ($p = 0.004$, 0.00) (Fig. 5A,B).

According to the MRI T2-weighted results, the mean signal intensity of NC group had barely changed throughout the study (Fig. 5C,D). Signal intensity in the DO group decreased significantly shortly and continued to develop after the operation, while those of transplantation groups were significantly delayed. The change of MRI T2-weighted signal intensity was evaluated by RGI. For the DO, CE and CC groups the mean RGI were 0.56 ± 0.05, 0.58 ± 0.03 and 0.58 ± 0.04 at 4 weeks after surgery respectively ($p > 0.05$). At 4 weeks, discs in CE and CC groups showed stronger signal intensities than that in DO group. At 24 weeks, the mean RGI of CE and CC groups were 0.41 ± 0.03 and 0.47 ± 0.04 respectively ($p = 0.044$), and these two groups showed higher RGI compared to DO group (0.26 ± 0.03, $p = 0.006$, 0.003).

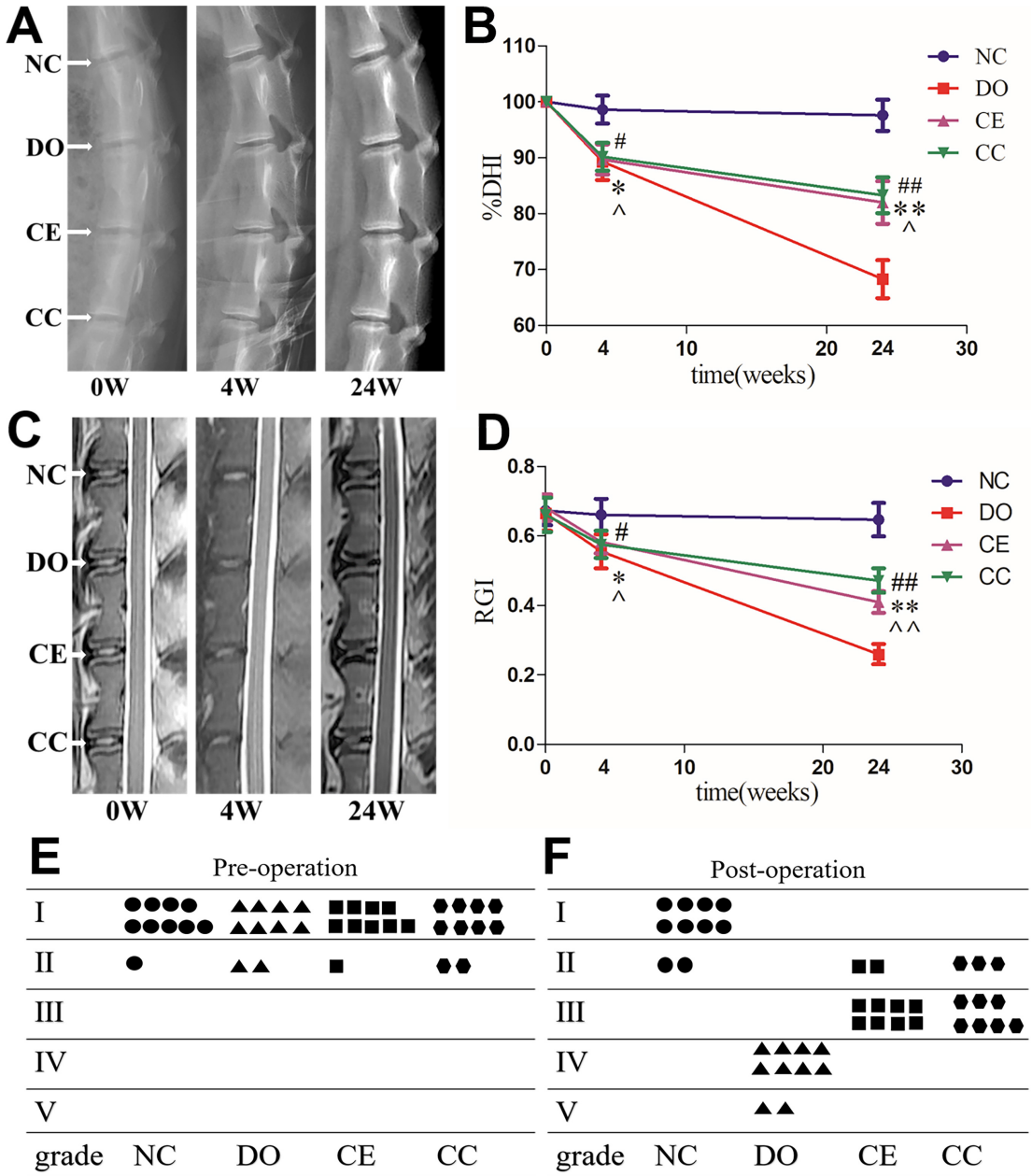

Fig. 5. Radiographic and MRI assessment. (A,C) Representative radiographic and MRI images at 0 week before, 4, and 24 weeks after operation in goats. (B,D) The change of disc height index (DHI) and relative grey index (RGI) at 4 and 24 weeks after operation. All the data represent mean ± SD, n = 10. '&' refers to NC group compared to DO group. '#', '*' refers to CE and CC groups compared to DO group respectively; '^' refers to CE group compared to CC group. #, *, ^, = $p > 0.05$; &, ##, **, = $p < 0.01$; ^^, = $p < 0.05$. (E,F) Pfirrmann grading of IVD degeneration in T2-weighted images. (E) Discs showed no degeneration in all groups before the operation. (F) There was significantly lower grading of MRI in the CE and CC groups compared with DO group at 24 weeks after operation ($p < 0.05$).

The Pfirrmann classification analysis showed that no obvious disc degeneration in all groups before the operation (Fig. 5E). There was no significant difference between the Pfirrmann classification of CE group and CC group (p = 1.00), which was significantly lower than that of DO group (p = 0.021, 0.01), but all of them were significantly higher compared with the NC group at 24 weeks after operation ($p < 0.05$) (Fig. 5F). Together, the analysis of imaging results shows that enriched BMA matrix and cultured BMSCs matrix transplantation can effectively maintain the IVD height and delay degeneration of the discs.

3.5 Biomechanical Analysis

We further compared the biomechanical effect from the three operated discs (DO, CE, and CC groups) and intact disc (NC group) at 24 weeks after operation. As shown in Fig. 3, the mean ROM of flexion-extension and left-right bending in the DO, CE and CC groups were 13.3 $\pm$ 1.2, 16.2 $\pm$ 1.8, 16.8 $\pm$ 1.5 degree and 7.6 $\pm$ 0.9, 11.8 $\pm$ 1.7, 12.5 $\pm$ 1.3 degree respectively, which of them significantly decreased compared with those of the NC group (18.2 $\pm$ 1.8, 14.4 $\pm$ 1.4 degree) (p = 0.013, 0.035, 0.042 and p = 0.00, 0.040, 0.037). The ROM of flexion-extension and left-right bending in the CE or CC group showed significantly less reduction compared with the DO group (p = 0.038, 0.041 and p = 0.015, 0.010). No significant differences were seen between CE and CC groups. The ROM of left-right rotation was 4.0 $\pm$ 0.7, 3.7 $\pm$ 0.5, 3.7 $\pm$ 0.6 and 3.8 $\pm$ 0.6 degree in the NC, DO, CE and CC groups respectively, however, there was not statistically different among them ($p > 0.05$). The result showed that the enriched BMA matrix and cultured BMSCs matrix transplanted into the discs maintained the stability of the degenerative IVD.

3.6 Macroscopic Findings

Gross observation of the lumbar spine showed that the fibrous connective tissue at the incision of AF in the CE and CC groups was rich, tough, and well repaired. However, the DO group had less connective tissue at the incision of the AF, and it was depressed and poorly repaired. The condition of NP and AF could be observed from the macroscopic view of freshly dissected IVD samples (Fig. 6A). In the DO group, in DO group, the NP and part of the AF tissue were black and yellow with severe degeneration. The CE and CC groups showed mild changes in NP tissue compared to the intact NC group. There are no NP protrusions in the discs of the CE and CC groups. Nine goats were assessed, showing that the histological grades of the discs in the CE and CC groups were mainly 2–3 grades, and that in DO group were mainly 4–5 grades. There was no significant difference in the grade of the discs between the CE and CC groups (p = 1.00), but both were lower than those of the DO group (p = 0.043, 0.024). Discs in NC group maintained grade 0 throughout the study (Fig. 6C).

3.7 Tracking of Transplanted BMSCs in IVD and Histological Analysis

In this study, GFP-labeled BMSCs combined with gelatin sponge matrix were transplanted into the IVD in the CC group. The discs of three goats were used to detect the tracking of transplanted BMSCs by fluorescence microscopy. As shown in **Supplementary Fig. 3D**, the fluorescence microscopy confirmed the tracking of the GFP-labeled BMSCs in the discs of the CC group.

No GFP-positive cells were observed in the discs of the DO or CE group (**Supplementary Fig. 3C**). The results showed that the GFP-labeled BMSCs was successfully implanted into the IVD and grew in the CC group.

H&E, Safranin O and Sirius red staining revealed that compared with the DO group, the structure of NP tissue in CE and the CC group was more complete, the cell proliferation was more active, and the extracellular matrix was more abundant (Fig. 7A). HE staining of the mid-coronal sections showed that disc height was well maintained in NC, CE and CC groups, whereas disc narrowing was obvious in DO group (Fig. 7B). The immunohistochemical staining of NP tissue in transversal sections indicated that the staining intensity of NP in the CE and CC groups was strong positive in aggrecan and type II collagen, while the staining intensity in the DO group was weak or intermediate positive (Fig. 7C).

3.8 Result of Gene Expression Analysis

For quantitative analysis the NP matrix, RT-PCR was used to measure the levels of aggrecan, type II collagen, type I collagen, and SOX-9 in the NC, DO, CE, and CC groups. As shown in Fig. 7D, the levels of aggrecan, type II collagen, and SOX-9 mRNAs were decreased in the DO, CE, and CC groups as compared with the NC group, while the type I collagen expression was significantly increased in the DO, CE, and CC groups ($p < 0.05$). Importantly, we found that the levels of aggrecan, type II collagen, and SOX-9 mRNAs were significantly higher in the CE and CC groups than those in the DO group, and the type I collagen expression was significantly lower in the CE and CC groups than that in the DO group ($p < 0.05$). Together, the results show that compared with the DO group, transplantation groups (CE group and CC group) increased the expression of aggrecan, type II collagen, and SOX-9, especially in CC group.

4. Discussion

IVD are avascular structures and their lack of oxygen and nutrient supply presents a substantial challenge for self-directed tissue repair [47]. IVD defects produced by discectomy may result in progressive degeneration, recurrence of disc herniation, and chronic pain. In the present study, we developed a biological approach to repair IVD defects following lumbar discectomy in goat models by implanting gelatin sponges seeded with autologous bone-marrow derived cells into the defect site before suturing and sealing. This preclinical proof-of-concept study demonstrated the feasibility and effectiveness of biomaterial and cell-based therapies for the repair of IVD defects.

Hydrogel materials are widely used in tissue repair due to the characteristics of high hydrophilicity, biocompatibility, and adjustable three-dimensional network mimicking extracellular matrix. The injectable hydrogel is of particular interest from a clinical point of view, as they can be injected as a liquid together with stem cells directly into the disc site in a minimally invasive way followed by gelation [44,48–51]. However, the hydrogel materials are gen-

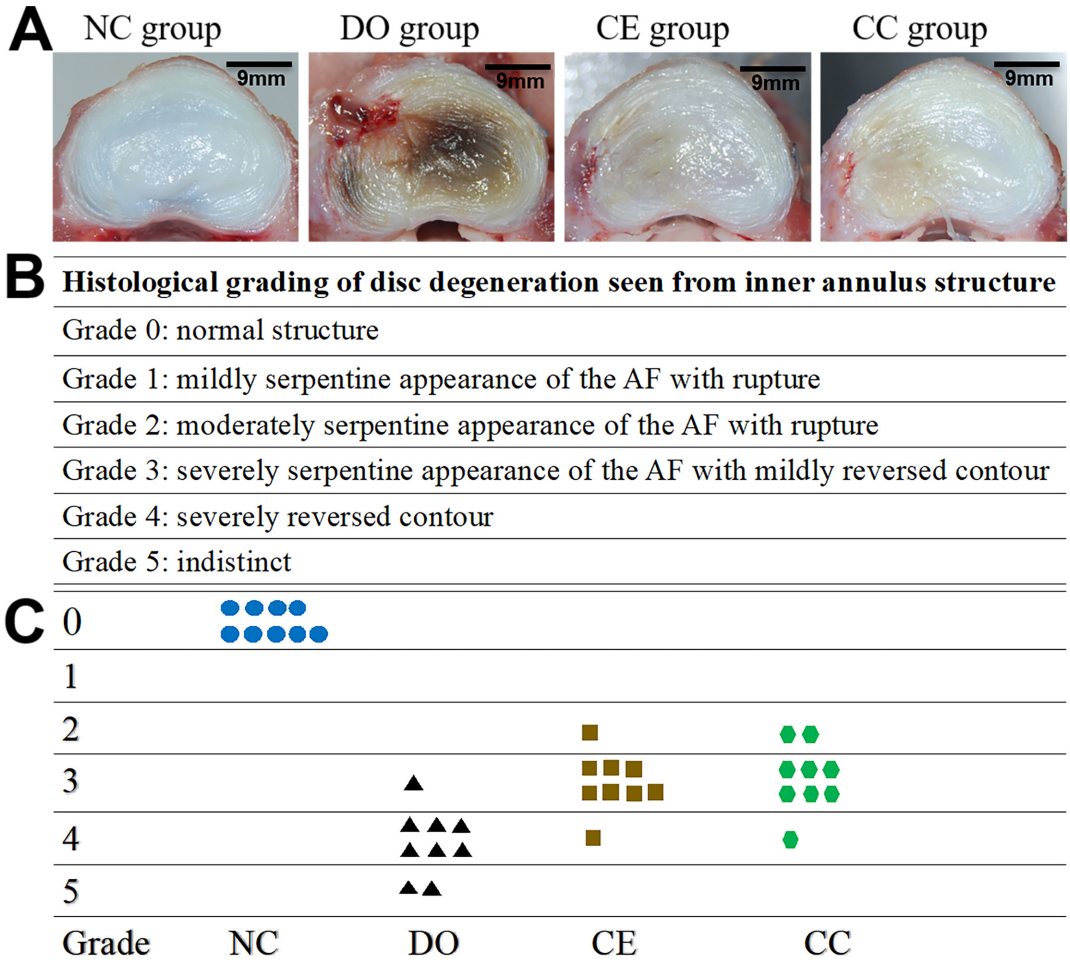

Fig. 6. Histological grading for assessment of IVD repair. (A) Representative macroscopic view of discs in four groups at 24 weeks. (B) The histological grading system for disc degeneration that focuses on morphological change in the inner annulus fibrosus structure was used in this study. (C) Histological grades were used to evaluate discs in the four groups at 24 weeks. There was no significant difference in histological grade between CE and CC groups ($p = 1.0$), but they were significantly lower than DO groups ($p < 0.05$).

erally not porous matrix structures, which were not suitable for cell enrichment in this study. The gelatin sponge is a three-dimensional porous structure, which is conducive to the smooth passage of BMA and the retention of target cells on the gelatin sponge. But, they are very soft when exposed to water and cannot provide mechanical support by themselves. However, through this experiment, the transplantation of enriched BMA-matrix or cultured BMSCs-matrix to repair the disc defect after discectomy can delay the degeneration of IVD and maintain a good height and mobility of IVD. The hydrogel has fluid properties, and the stem cell impregnated hydrogels is easily injected into the degenerated NP through a fine needle, with little effect on the AF, which could restore disc height, thus providing immediate pain relief, whilst delivery of MSCs provides gradual regeneration. The hydrogel appears to be more suitable for the repair of early to midstages of disc degeneration, with intact AF [49]. The main role of the gelatin sponge in this experiment is to retain the target cells during the enrichment process, and act as a carrier to reduce the leakage of the cells. However, the mechanical strength of gelatin sponge is insufficient. In the future, gelatin sponge with higher mechanical strength is developed for intervertebral disc repair, which can provide better space for the growth and differentiation of transplanted cells, and the effect may be better.

Cell-based therapy is a promising reparative strategy for IVD regeneration. Given the insufficient stem cell or IVD cell number and sources, cells culture-expanded method was widely adopted for cell transplantation. However, cell culture in vitro is controversy in clinical application, which may increase the cost of the patients and the risk of differentiate abnormality and microorganism contamination [52,53]. SCR is a non-cultivation technique, which can help avoid some ethical and physico-chemical influences of *in vitro* cell expansion. Muschler *et al.* [25,34] first reported a SCR method that used a composite matrix prepa-

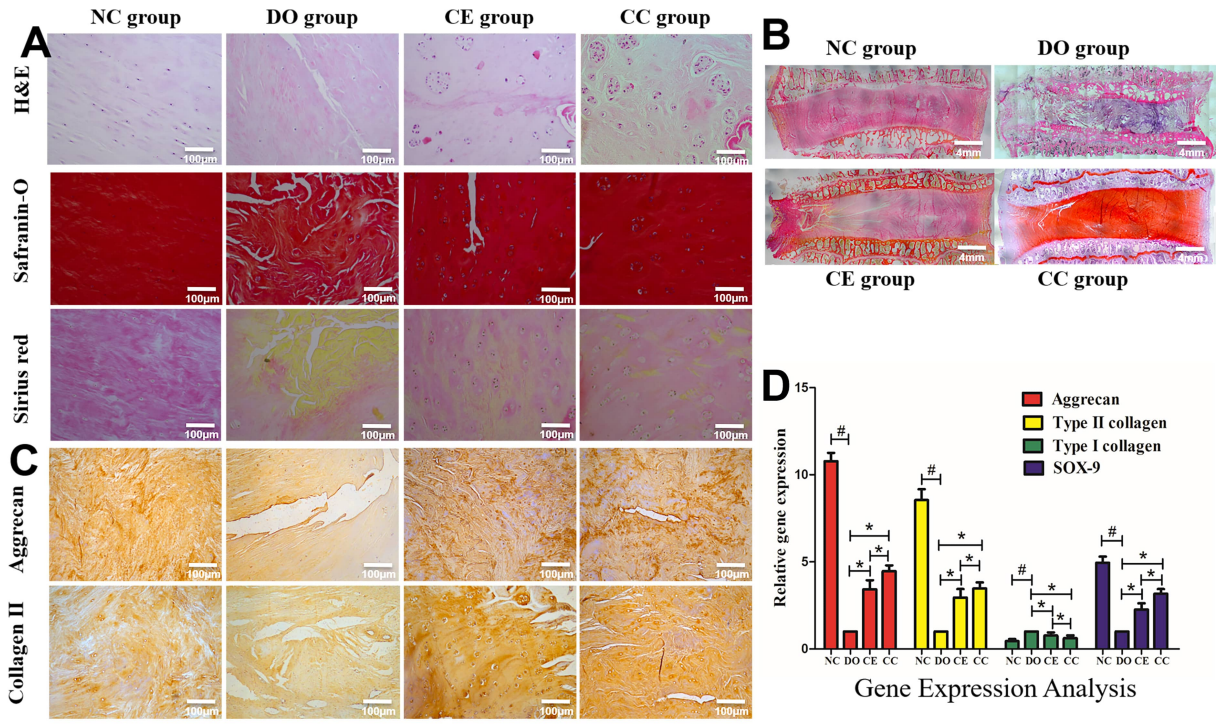

Fig. 7. Histological and real-time PCR analysis. (A) H&E, Safranin O and Sirius red staining of NP in the transversal plane. (B) the intact IVD of mid-coronal sections were stained with HE staining. (C) The immunohistochemical staining for aggrecan and type II collagen. (D) Real-time PCR analysis. The results showed that aggrecan, type II collagen, and SOX-9 mRNA expression markedly increased in discs from the CE and CC group compared with the DO groups. Bar plots are shown as means ± SD, n = 9. '#' refers to NC group compared to DO group. '*' refers to the comparison among CE, CC and DO groups; #, *, = $p < 0.05$.

ration loaded with bone-marrow derived cells for lumbar fusion surgery, which indicated that cell-enriched matrix grafts were capable of delivering a mean of 2.3-fold more cells and approximately 5.6-fold more progenitor cells than matrix mixed directly with bone marrow. In the present study, we showed that the adhesion number of multiple nucleated cells and the target cells to gelatin sponges was approximately 6.4-fold and 4.2-fold, respectively, when compared to BMA (Fig. 4J). Additionally, MSCs can be concentrated and rapidly combined with scaffolds using SCR techniques. SEM images showed the enriched cells could adhere to the porous walls of gelatin sponges. Plastic-adherence is an important feature of MSCs [54]. After enriched BMA-matrices were cultured for 11 days, a large number of CFU-F grew adherently, which indirectly reflects the number of progenitor cells [37,55,56]. Moreover, MSC surface markers were detected by flow cytometry [55], which showed that BGP was more conducive to enrichment ability. These results indicated that BGP effectively retained MSCs within the gelatin sponges and maintained their stemness activity. Furthermore, the enrichment process totaled 5 min and this simplistic and timesaving procedure was appropriate for critical operation times. Our results indicated that SCR technology was a valid approach for concentrating cell numbers whilst cell activity could be preserved by using cell-carrier combinations.

Cell enrichment technology combined with implant materials to concentrate bone marrow has been used in spinal fusion [25,34] and bone defect [35] treatments. In an open label pilot study, 26 patients with chronic back pain due to degenerative disc disease (median age 40 years; range 18–61) received autologous bone marrow concentrated intra-disc injections and all subjects presented a substantial reduction in pain [57]. However, few previous researches have attempted to use enriched BMA to repair surgical IVD defects. Our results, imaging analysis, and histological assessment showed that both enriched MSCs and cultured BMSCs combined with gelatin sponge cubes have the potential to repair IVD defects, maintain IVD height for 24 weeks, and may delayed IVD degeneration. Although SCR techniques do not provide the same number of MSCs as cell culture expansion techniques, they still produced efficacious therapeutic effects. We speculate that cytokines/chemokines within the bone marrow play a contributing role to this outcome. Compared with *in vitro* culture of BMSCs, MSCs enrichment by BGP is facile, faster, and more convenient for clinical point-of-use. Our study showed the feasibility and safety of enriched MSCs combined with gelatin sponge cubes for repairing IVD defects in large animal models, demonstrating the strong potential of this method for clinical use in patients with IVD defects.

MSCs have the capacity for multidirectional differentiation. A two-way communication has been observed wherein MSCs interact with nucleus pulposus cells (NPCs) [58,59]. The paracrine environmental signalling from NPCs instructs MSCs to differentiate toward NPC-like cell lineages [60–62]. Concurrently, MSC signalling can influence the activity of NPCs [11,63]. However, when MSCs leak from the IVD defect or injection site due to high intradisc pressure, considerable ossification can occur [64,65]. This suggests the significance of developing appropriate cell carriers and effective approaches to prevent cell leakage and the associated osteophyte formation before MSCs-based therapies can be applied in clinical settings. In this study, we sought to circumvent cell leakage issues by transplanting gelatin sponges seeded with autologous MSCs, and this was followed by AF suture to close the breach. Our results showed that there was no obvious indications of osteophyte or heterotopic ossification formation. Potential reasons for preventing osteophyte formation may be: (i) enhanced cell retention *in situ* by using clinically used gelatin sponges as cell-carriers, providing enhanced cell adhesion; (ii) physical closure of AF defects by suturing to prevent leakage of the transplanted cell-carrier; (iii) closure of disc defects reduced immuno-inflammatory responses otherwise invoked by the exposed disc; (iv) a reduced foreign body reaction and inflammatory cell interferences through use of autologous MSCs transplantation. Therefore, our strategy developed for IVD repair demonstrated safe and effective applicability of cell-carrier therapies for intra-disc delivery. Furthermore, some preclinical and clinical studies demonstrated that MSCs injection therapy is an effective treatment to retard disc degeneration and relieve pain. Despite tremendous research efforts, MSCs therapy to repair the IVD still has controversy and considerable challenges. The hostility of the microenvironment in IVDD niches may limits the viability and functionality of the transplanted MSCs. And the safety and efficacy of cell-based therapy is still controversial [66,67].

In order to evaluate the effectiveness of the developed strategies for IVD tissue repair and regeneration, it is important to use appropriate animal models. Recent advancements in biological repair strategies have shown successful preclinical outcomes *in vitro* and *in vivo* [27–31,68,69]. Long *et al*. [28] established a biopsy-type AF defect in an ovine cervical model to evaluate the in vivo response of a composite AF repair strategy. Shu *et al*. [70] group utilized an ovine IVDD model and intradiscal heterologous MSCs to determine therapeutic efficacy at early, late acute and chronic stages of IVDD. MSCs were intradiscal administered into the NP from the contralateral AF away from the annular lesion site. Results showed that the administered MSCs can interact with resident disc cells to initiate and coordinate the repair processes and prevented the extension of the AF defect and promoted the healing of outer AF defect. However, there are a limited number of studies that have established animal models that mimic the clinical post-surgery conditions in humans with LDH. Until now, only two studies have reported the use of injectable defect-filing hydrogels [71] and modified hyaluronic acid [72] to repair post-discectomy IVD defects in sheep models. In this context, we successfully established a discectomy-associated defect model in goats, which simulated the clinical circumstances. Indeed, in artiodactyls, the anatomical structure, size, biomechanical properties, and biochemical components of goat IVDs are relatively close to human IVDs, which make the animal better model to recapitulate human IVD pathophysiology [29,73]. Although goats are quadrupeds and do not share the upright characteristics of the human spine, the musculature of quadruped provides high muscle tension such that the pressure within lumbar IVDs is similar to the human intradiscal pressure [72,74]. This experimental was testing in a quadraped animal and human IVD loading is different. The animal model of upright walking needs further research.

Mechanical integrity is important for IVD function. IVD defects can cause loading disorders, resulting in progressive degeneration [75]. Therefore, repairing the IVD defect may restore mechanical compliance. In addition, IVDs load bearing is complex and dynamic. Dynamic biomechanical testing should be conducted to evaluate IVD repair. This study tested biomechanical functions of whole lumbar kinematics after repairing IVD defect *in vivo*, including the range of motion in flexion, extension, bending and rotation tests. Mechanical testing results demonstrated that the ROM of flexion-extension and left–right bending in defect repairing group were better than that in discectomy alone group. However, there were no statistical differences calculated in ROM of rotation due to the long distance from the rotation center to the edge of AF defect, and this is a limitation of utilizing quadruped animal models such as goats, which rarely exert spinal rotation motions. Thorpe *et al*. [49] reported that a thermally triggered hydrogel was injected into bovine NP tissue explants in a statically cultured model. Mechanical analysis showed that MSC and hydrogel injected NP tissue explants displayed similar mechanical properties to control group with no significant difference following 6 weeks in culture. Our study indirectly assessed the effect of treatment measures on IVD biomechanical function by detecting the ROM in the motion segments of spine, which is not as accurate as direct mechanical testing of the disc, which is a limitation of the study.

The anatomy and mechanical property of the 4 level IVDs may have some differences. It would have been better to systematically rotate the groups among the different level IVDs. The lumbar IVDs in each spine should be randomized to receive different treatment strategies to reduce the impact of differences in anatomical and mechanical properties at different levels. An additional limitation of our study was that the cells were harvested from normal healthy goats, and the goats themselves were in a healthy and active

state. In clinical settings, patients have a variety of compromising health conditions that can induce IVD degenerative states. An example setting wherein our approach is likely to be unsuitable is in elderly patients with severe degeneration of AF, resulting in heightened difficulty of suture and defect closure. Furthermore, MSCs fate after implantation was not a focus of our investigation. Lineage tracing and phenotypic evaluation are required in future investigations. This experimental only proved that the concentration of the target cells on the gelatin sponge increased after the BMA passed through the BGP. We currently have no direct evidence that cells adhere more readily to gelatin sponge scaffolds. This is a limitation of our study and requires further investigation.

5. Conclusions

This preclinical proof-of-concept study shows the feasibility and effectiveness of transplanting gelatin sponge seeded with autologous enriched MSCs into the disc defect after discectomy, and then suturing and sealing AF defect. To the authors knowledge, this in vivo study is the first to demonstrate the feasibility and effectiveness of IVD defect repair in goat lumbar model using enriched MSCs seeded gelatin sponge combined with AF suture. The present results indicate this novel reparative strategy could delay the progress of IVD degeneration and restore the extracellular matrix of IVD, imperative for maintaining disc height and biomechanical properties. Compared with culturing BM-SCs, the enrichment of MSCs with SCR technology at the point of operation, is a simpler, safer, and more time- and cost-economical approach. In light of the promising evidence from this investigation, the authors have commenced a human clinical trial using the same reparative strategy in patients with LDH by endoscopic discectomy (ClinicalTrials.gov NCT03002207). Overall, the combinatory approach of SCR technology with autologous MSC adhesion to gelatin sponges facilitated enhanced repair of IVD defects, restored biomechanical function, and minimized risk of cell-leakage and ossification. The results from this study showing a potential avenue toward clinical translation for IVD defect repair and prevention of disc degeneration in post-discectomy settings.

Abbreviations

IVD, intervertebral disc; SCR, selective cell retention; MSCs, mesenchymal stromal cells; BMA, bone marrow aspirate; NP, nucleus pulposus; IVDD, intervertebral disc degeneration; LDH, lumbar disc herniation; AF, annulus fibrosus; BM-MSCs, bone marrow-derived MSCs; ASCs, adipose-derived MSCs; UC-MSCs, umbilical cord-derived MSCs; MRI, magnetic resonance imaging; BGP, BONE GROWTH PROMOTER; PBS, phosphate buffered saline; GFP, green fluorescent protein; DHI, disc height index; EDTA, ethylenediamine tetraacetic acid; H&E, hematoxylin and eosin; DAB, diamino-benzidine; OCT, optimal cutting temperature; CFU-F, colonies forming unit-fibroblast; PCR, polymerase chain reaction; RT-PCR, real-time PCR; ROM, range of motion; SEM, scanning electron microscope; NPCs, nucleus pulposus cells.

Author Contributions

QY, LD and HX contributed equally to this work, participated in the design of the study, performed enrichment testing, cell culture and animal experiments, imaging detection, biomechanical testing and analysis, (immuno)histochemistry detection, microscopy analyses, acquisition, analysis and interpretation of results, and drafted the manuscript. BX conceptualized, designed the study and provided financial supports. QY, LD, HX, KZ, QL, HZ and YL helped with implement of animal surgery. KZ carried out the gene detection. QY, LD, HX, HZ and BX helped with statistical analysis. XM and BX provided technical, administrative and material support. BX supervised the study and helped to revise the manuscript. All authors read and approved the final manuscript.

Ethics Approval and Consent to Participate

Animal experiments were approved by the Animal Experiments Ethical Committee of Institute of Radiation Medicine Chinese Academy of Medical Sciences, Tianjin, China (approval number: IRM-DWLL-2020142).

Acknowledgment

We want to thank all research personnel for their contributory works. Thanks to Yeda Wan, Yi Cao and Nan Wang of the Radiology Department of Tianjin Hospital for their help in image detection and analysis.

Funding

This study was supported by the National Natural Science Foundation of China (82072491, 31900967, 31670983) and Natural Science Foundation of Tianjin (19JCQNJC09300).

Conflict of Interest

The authors declare no conflict of interest.

Supplementary Material

Supplementary material associated with this article can be found, in the online version, at https://doi.org/10.31083/j.fbl2704131.

References

[1] Balagué F, Mannion AF, Pellisé F, Cedraschi C. Clinical update: low back pain. The Lancet. 2007; 369: 726–728.

[2] Asch HL, Lewis PJ, Moreland DB, Egnatchik JG, Yu YJ, Clabeaux DE, *et al*. Prospective multiple outcomes study of outpatient lumbar microdiscectomy: should 75 to 80% success rates be the norm? Journal of Neurosurgery. 2002; 96: 34–44.

[3] Weinstein JN, Lurie JD, Tosteson TD, Skinner JS, Hanscom B, Tosteson ANA, *et al*. Surgical vs nonoperative treatment for lumbar disk herniation: the Spine Patient Outcomes Research Trial (SPORT) observational cohort. Journal of the American Medical Association. 2006; 296: 2451–2459.
[4] Bailey A, Araghi A, Blumenthal S, Huffmon GV. Prospective, multicenter, randomized, controlled study of anular repair in lumbar discectomy: two-year follow-up. Spine. 2013; 38: 1161–1169.
[5] Parker SL, Grahovac G, Vukas D, Vilendecic M, Ledic D, McGirt MJ, *et al*. Effect of an Annular Closure Device (Barricaid) on Same-Level Recurrent Disk Herniation and Disk Height Loss after Primary Lumbar Discectomy: Two-year Results of a Multicenter Prospective Cohort Study. Clinical Spine Surgery. 2016; 29: 454–460.
[6] Tavakoli J, Diwan AD, Tipper JL. Advanced Strategies for the Regeneration of Lumbar Disc Annulus Fibrosus. International Journal of Molecular Sciences. 2020; 21: 4889.
[7] Bailey A, Araghi A, Blumenthal S, Huffmon GV. Anular Repair After Lumbar Discectomy Did Not Reduce the Need for Reherniation Surgery. Journal of Bone and Joint Surgery-Series A. 2014; 96: 870.
[8] Guardado AA, Baker A, Weightman A, Hoyland JA, Cooper G. Lumbar Intervertebral Disc Herniation: Annular Closure Devices and Key Design Requirements. Bioengineering. 2022; 9: 47.
[9] Ganey T, Libera J, Moos V, Alasevic O, Fritsch K, Meisel HJ, *et al*. Disc chondrocyte transplantation in a canine model: a treatment for degenerated or damaged intervertebral disc. Spine. 2003; 28: 2609–2620.
[10] de Vries S, Doeselaar MV, Meij B, Tryfonidou M, Ito K. Notochordal Cell Matrix as a Therapeutic Agent for Intervertebral Disc Regeneration. Tissue Engineering Part A. 2019; 25: 830–841.
[11] Shim E, Lee J, Kim D, Kim SK, Jung B, Choi E, *et al*. Autogenous Mesenchymal Stem Cells from the Vertebral Body Enhance Intervertebral Disc Regeneration via Paracrine Interaction: an in Vitro Pilot Study. Cell Transplantation. 2016; 25: 1819–1832.
[12] Sakai D, Andersson GB. Stem cell therapy for intervertebral disc regeneration: obstacles and solutions. Nature Reviews Rheumatology. 2015; 11: 243–256.
[13] Stoyanov JV, Gantenbein-Ritter B, Bertolo A, Aebli N, Baur M, Alini M, *et al*. Role of hypoxia and growth and differentiation factor-5 on differentiation of human mesenchymal stem cells towards intervertebral nucleus pulposus-like cells. European Cells and Materials. 2011; 21: 533–547.
[14] Sakai D, Mochida J, Iwashina T, Hiyama A, Omi H, Imai M, *et al*. Regenerative effects of transplanting mesenchymal stem cells embedded in atelocollagen to the degenerated intervertebral disc. Biomaterials. 2006; 27: 335–345.
[15] Clarke LE, McConnell JC, Sherratt MJ, Derby B, Richardson SM, Hoyland JA. Growth differentiation factor 6 and transforming growth factor-beta differentially mediate mesenchymal stem cell differentiation, composition, and micromechanical properties of nucleus pulposus constructs. Arthritis Research and Therapy. 2014; 16: R67.
[16] Wang YT, Wu XT, Wang F. Regeneration potential and mechanism of bone marrow mesenchymal stem cell transplantation for treating intervertebral disc degeneration. Journal of Orthopaedic Science. 2010; 15: 707–719.
[17] Binch ALA, Fitzgerald JC, Growney EA, Barry F. Cell-based strategies for IVD repair: clinical progress and translational obstacles. Nature Reviews Rheumatology. 2021; 17: 158–175.
[18] Smith LJ, Silverman L, Sakai D, Le Maitre CL, Mauck RL, Malhotra NR, *et al*. Advancing cell therapies for intervertebral disc regeneration from the lab to the clinic: Recommendations of the ORS spine section. JOR Spine. 2018; 1: e1036.
[19] Schol J, Sakai D. Cell therapy for intervertebral disc herniation and degenerative disc disease: clinical trials. International Orthopaedics. 2019; 43: 1011–1025.
[20] Meisel HJ, Siodla V, Ganey T, Minkus Y, Hutton WC, Alasevic OJ. Clinical experience in cell-based therapeutics: disc chondrocyte transplantation a treatment for degenerated or damaged intervertebral disc. Biomolecular Engineering. 2007; 24: 5–21.
[21] Amirdelfan K, Bae H, McJunkin T, DePalma M, Kim K, Beckworth WJ, *et al*. Allogeneic mesenchymal precursor cells treatment for chronic low back pain associated with degenerative disc disease: a prospective randomized, placebo-controlled 36-month study of safety and efficacy. Spine Journal. 2020; 21: 212–230.
[22] Yoshikawa T, Ueda Y, Miyazaki K, Koizumi M, Takakura Y. Disc regeneration therapy using marrow mesenchymal cell transplantation: a report of two case studies. Spine. 2010; 35: E475–E480.
[23] Mautner K, Bowers R, Easley K, Fausel Z, Robinson R. Functional Outcomes Following Microfragmented Adipose Tissue Versus Bone Marrow Aspirate Concentrate Injections for Symptomatic Knee Osteoarthritis. Stem Cells Translational Medicine. 2019; 8: 1149–1156.
[24] Yousef MAA, La Maida GA, Misaggi B. Long-term Radiological and Clinical Outcomes after Using Bone Marrow Mesenchymal Stem Cells Concentrate Obtained with Selective Retention Cell Technology in Posterolateral Spinal Fusion. Spine. 2017; 42: 1871–1879.
[25] Muschler GF, Matsukura Y, Nitto H, Boehm CA, Valdevit AD, Kambic HE, *et al*. Selective retention of bone marrow-derived cells to enhance spinal fusion. Clinical Orthopaedics and Related Research. 2005; 432: 242–251.
[26] Bruder SP, Jaiswal N, Ricalton NS, Mosca JD, Kraus KH, Kadiyala S. Mesenchymal stem cells in osteobiology and applied bone regeneration. Clinical Orthopaedics and Related Research. 1998; 355: S247–S256.
[27] Hussain I, Sloan SR, Wipplinger C, Navarro-Ramirez R, Zubkov M, Kim E, *et al*. Mesenchymal Stem Cell-Seeded High-Density Collagen Gel for Annular Repair: 6-Week Results from in Vivo Sheep Models. Neurosurgery. 2019; 85: E350–E359.
[28] Long RG, Ferguson SJ, Benneker LM, Sakai D, Li Z, Pandit A, *et al*. Morphological and biomechanical effects of annulus fibrosus injury and repair in an ovine cervical model. JOR Spine. 2020; 3: e1074.
[29] Gullbrand SE, Ashinsky BG, Bonnevie ED, Kim DH, Engiles JB, Smith LJ, *et al*. Long-term mechanical function and integration of an implanted tissue-engineered intervertebral disc. Science Translational Medicine. 2018; 10: eaau0670.
[30] Bendtsen M, Bünger CE, Zou X, Foldager C, Jørgensen HS. Autologous Stem Cell Therapy Maintains Vertebral Blood Flow and Contrast Diffusion through the Endplate in Experimental Intervertebral Disc Degeneration. Spine. 2011; 36: E373–E379.
[31] Zhang Y, Tao H, Gu T, Zhou M, Jia Z, Jiang G, *et al*. The effects of human Wharton's jelly cell transplantation on the intervertebral disc in a canine disc degeneration model. Stem Cell Research and Therapy. 2015; 6: 154.
[32] Hiraishi S, Schol J, Sakai D, Nukaga T, Erickson I, Silverman L, *et al*. Discogenic cell transplantation directly from a cryopreserved state in an induced intervertebral disc degeneration canine model. JOR Spine. 2018; 1: e1013.
[33] Xu X, Hu J, Lu H. Histological observation of a gelatin sponge transplant loaded with bone marrow-derived mesenchymal stem cells combined with platelet-rich plasma in repairing an annulus defect. PLoS ONE. 2017; 12: e0171500.
[34] Muschler GF, Nitto H, Matsukura Y, Boehm C, Valdevit A, Kambic H, *et al*. Spine fusion using cell matrix composites en-

riched in bone marrow-derived cells. Clinical Orthopaedics and Related Research. 2003; 407: 102–118.
[35] Jacobsen K, Szczepanowski K, Al-Zube LA, Kim J, Lin SS. The Role of Intraoperative Bone Marrow Aspirate Stem Cell Concentration as a Bone Grafting Technique. Techniques in Foot and Ankle Surgery. 2008; 7: 84–89.
[36] Hou T, Li Z, Luo F, Xie Z, Wu X, Xing J, *et al*. A composite demineralized bone matrix-self assembling peptide scaffold for enhancing cell and growth factor activity in bone marrow. Biomaterials. 2014; 35: 5689–5699.
[37] Hegde V, Shonuga O, Ellis S, Fragomen A, Kennedy J, Kudryashov V, *et al*. A prospective comparison of 3 approved systems for autologous bone marrow concentration demonstrated nonequivalency in progenitor cell number and concentration. Journal of Orthopaedic Trauma. 2014; 28: 591–598.
[38] Gronthos S, Zannettino ACW, Hay SJ, Shi S, Graves SE, Kortesidis A, *et al*. Molecular and cellular characterisation of highly purified stromal stem cells derived from human bone marrow. Journal of Cell Science. 2003; 116: 1827–1835.
[39] Oehme D, Goldschlager T, Rosenfeld J, Danks A, Ghosh P, Gibbon A, *et al*. Lateral Surgical Approach to Lumbar Intervertebral Discs in an Ovine Model. The Scientific World Journal. 2012; 2012: 873726.
[40] Masuda K, Imai Y, Okuma M, Muehleman C, Nakagawa K, Akeda K, *et al*. Osteogenic Protein-1 Injection into a Degenerated Disc Induces the Restoration of Disc Height and Structural Changes in the Rabbit Anular Puncture Model. Spine. 2006; 31: 742–754.
[41] Han B, Zhu K, Li F, Xiao Y, Feng J, Shi Z, *et al*. A Simple Disc Degeneration Model Induced by Percutaneous Needle Puncture in the Rat Tail. Spine. 2008; 33: 1925–1934.
[42] Pfirrmann CW, Metzdorf A, Zanetti M, Hodler J, Boos N. Magnetic resonance classification of lumbar intervertebral disc degeneration. Spine. 2001; 26: 1873–1878.
[43] Nishimura K, Mochida J. Percutaneous reinsertion of the nucleus pulposus. An experimental study. Spine. 1998; 23: 1531–1539.
[44] Zeng Y, Chen C, Liu W, Fu Q, Han Z, Li Y, *et al*. Injectable microcryogels reinforced alginate encapsulation of mesenchymal stromal cells for leak-proof delivery and alleviation of canine disc degeneration. Biomaterials. 2015; 59: 53–65.
[45] Reno C, Marchuk L, Sciore P, Frank CB, Hart DA. Rapid isolation of total RNA from small samples of hypocellular, dense connective tissues. BioTechniques. 1997; 22: 1082–1086.
[46] Livak KJ, Schmittgen TD. Analysis of relative gene expression data using real-time quantitative PCR and the 2(-Delta Delta C(T)) Method. Methods. 2001; 25: 402–408.
[47] Raj PP. Intervertebral disc: anatomy-physiology-pathophysiology-treatment. Pain Practice. 2008; 8: 18–44.
[48] Russo F, Ambrosio L, Peroglio M, Guo W, Wangler S, Gewiess J, *et al*. A hyaluronan and platelet-rich plasma hydrogel for mesenchymal stem cell delivery in the intervertebral disc: an organ culture study. International Journal of Molecular Sciences. 2021; 22: 2963.
[49] Thorpe AA, Dougill G, Vickers L, Reeves ND, Sammon C, Cooper G, *et al*. Thermally triggered hydrogel injection into bovine intervertebral disc tissue explants induces differentiation of mesenchymal stem cells and restores mechanical function. Acta Biomaterialia. 2017; 54: 212–226.
[50] Friedmann A, Baertel A, Schmitt C, Ludtka C, Milosevic J, Meisel HJ, *et al*. Intervertebral Disc Regeneration Injection of a Cell-Loaded Collagen Hydrogel in a Sheep Model. International Journal of Molecular Sciences. 2021; 22: 4248.
[51] Schmitt C, Radetzki F, Stirnweiss A, Mendel T, Ludtka C, Friedmann A, *et al*. Long-term pre-clinical evaluation of an injectable chitosan nanocellulose hydrogel with encapsulated adipose-derived stem cells in an ovine model for IVD regeneration. Journal of Tissue Engineering and Regenerative Medicine. 2021; 15: 660–673.
[52] Pettine KA, Suzuki RK, Sand TT, Murphy MB. Autologous bone marrow concentrate intradiscal injection for the treatment of degenerative disc disease with three-year follow-up. International Orthopaedics. 2017; 41: 2097–2103.
[53] Ukeba D, Yamada K, Tsujimoto T, Ura K, Nonoyama T, Iwasaki N, *et al*. Bone Marrow Aspirate Concentrate Combined with in Situ Forming Bioresorbable Gel Enhances Intervertebral Disc Regeneration in Rabbits. Journal of Bone and Joint Surgery. 2021; 103: e31.
[54] Dominici M, Le Blanc K, Mueller I, Slaper-Cortenbach I, Marini F, Krause D, *et al*. Minimal criteria for defining multipotent mesenchymal stromal cells. The International Society for Cellular Therapy position statement. Cytotherapy. 2006; 8: 315–317.
[55] Tondreau T, Lagneaux L, Dejeneffe M, Delforge A, Massy M, Mortier C, *et al*. Isolation of BM mesenchymal stem cells by plastic adhesion or negative selection: phenotype, proliferation kinetics and differentiation potential. Cytotherapy. 2004; 6: 372–379.
[56] Hustedt JW, Jegede KA, Badrinath R, Bohl DD, Blizzard DJ, Grauer JN. Optimal aspiration volume of vertebral bone marrow for use in spinal fusion. Spine Journal. 2013; 13: 1217–1222.
[57] Pettine KA, Murphy MB, Suzuki RK, Sand TT. Percutaneous injection of autologous bone marrow concentrate cells significantly reduces lumbar discogenic pain through 12 months. Stem Cells. 2015; 33: 146–156.
[58] Ho G, Leung VYL, Cheung KMC, Chan D. Effect of severity of intervertebral disc injury on mesenchymal stem cell-based regeneration. Connective Tissue Research. 2008; 49: 15–21.
[59] Paesold G, Nerlich AG, Boos N. Biological treatment strategies for disc degeneration: potentials and shortcomings. European Spine Journal. 2007; 16: 447–468.
[60] Crevensten G, Walsh AJ, Ananthakrishnan D, Page P, Wahba GM, Lotz JC, *et al*. Intervertebral disc cell therapy for regeneration: mesenchymal stem cell implantation in rat intervertebral discs. Annals of Biomedical Engineering. 2004; 32: 430–434.
[61] Sakai D, Mochida J, Yamamoto Y, Nomura T, Okuma M, Nishimura K, *et al*. Transplantation of mesenchymal stem cells embedded in Atelocollagen gel to the intervertebral disc: a potential therapeutic model for disc degeneration. Biomaterials. 2003; 24: 3531–3541.
[62] Sakai D, Mochida J, Iwashina T, Watanabe T, Nakai T, Ando K, *et al*. Differentiation of mesenchymal stem cells transplanted to a rabbit degenerative disc model: potential and limitations for stem cell therapy in disc regeneration. Spine. 2005; 30: 2379–2387.
[63] Chen S, Zhao L, Deng X, Shi D, Wu F, Liang H, *et al*. Mesenchymal Stem Cells Protect Nucleus Pulposus Cells from Compression-Induced Apoptosis by Inhibiting the Mitochondrial Pathway. Stem Cells International. 2017; 2017: 9843120.
[64] Vadalà G, Sowa G, Hubert M, Gilbertson LG, Denaro V, Kang JD. Mesenchymal stem cells injection in degenerated intervertebral disc: cell leakage may induce osteophyte formation. Journal of Tissue Engineering and Regenerative Medicine. 2012; 6: 348–355.
[65] Chik TK, Ma XY, Choy TH, Li YY, Diao HJ, Teng WK, *et al*. Photochemically crosslinked collagen annulus plug: a potential solution solving the leakage problem of cell-based therapies for disc degeneration. Acta Biomaterialia. 2013; 9: 8128–8139.
[66] Loibl M, Wuertz-Kozak K, Vadala G, Lang S, Fairbank J, Urban JP. Controversies in regenerative medicine: should intervertebral disc degeneration be treated with mesenchymal stem cells? JOR Spine. 2019; 2: e1043.
[67] Vickers L, Thorpe AA, Snuggs J, Sammon C, Le Maitre CL.

Mesenchymal stem cell therapies for intervertebral disc degeneration: Consideration of the degenerate niche. JOR Spine. 2019; 2: e1055.

[68] Watanabe T, Sakai D, Yamamoto Y, Iwashina T, Serigano K, Tamura F, *et al*. Human nucleus pulposus cells significantly enhanced biological properties in a coculture system with direct cell-to-cell contact with autologous mesenchymal stem cells. Journal of Orthopaedic Research. 2010; 28: 623–630.

[69] Nukaga T, Sakai D, Tanaka M, Hiyama A, Nakai T, Mochida J. Transplantation of activated nucleus pulposus cells after cryopreservation: efficacy study in a canine disc degeneration model. European Cells and Materials. 2016; 31: 95–106.

[70] Shu CC, Dart A, Bell R, Dart C, Clarke E, Smith MM, *et al*. Efficacy of administered mesenchymal stem cells in the initiation and co-ordination of repair processes by resident disc cells in an ovine (Ovis aries) large destabilizing lesion model of experimental disc degeneration. JOR Spine. 2018; 1: e1037.

[71] Tsujimoto T, Sudo H, Todoh M, Yamada K, Iwasaki K, Ohnishi T, *et al*. An acellular bioresorbable ultra-purified alginate gel promotes intervertebral disc repair: a preclinical proof-of-concept study. EBioMedicine. 2018; 37: 521–534.

[72] Sloan SR Jr, Wipplinger C, Kirnaz S, Navarro-Ramirez R, Schmidt F, McCloskey D, *et al*. Combined nucleus pulposus augmentation and annulus fibrosus repair prevents acute intervertebral disc degeneration after discectomy. Science Translational Medicine. 2020; 12: eaay2380.

[73] Zhang Y, Drapeau S, Howard SA, Thonar EJMA, Anderson DG. Transplantation of Goat Bone Marrow Stromal Cells to the Degenerating Intervertebral Disc in a Goat Disc Injury Model. Spine. 2011; 36: 372–377.

[74] Reitmaier S, Schmidt H, Ihler R, Kocak T, Graf N, Ignatius A, *et al*. Preliminary investigations on intradiscal pressures during daily activities: an in vivo study using the merino sheep. PLoS ONE. 2013; 8: e69610.

[75] Bonnevie ED, Gullbrand SE, Ashinsky BG, Tsinman TK, Elliott DM, Chao PG, *et al*. Aberrant mechanosensing in injured intervertebral discs as a result of boundary-constraint disruption and residual-strain loss. Nature Biomedical Engineering. 2019; 3: 998–1008.